Results from a Global Ocean Model in the Western Tropical Pacific

Harley HURLBURT[1], John KINDLE[1], E. Joseph METZGER[1] and Alan WALLCRAFT[2]

[1] *JAYCOR;* [2] *NORDA*
Stennis Space Center, MS 39529 - U.S.A.

1. Introduction.

The circulation of the western equatorial Pacific is examined using two NORDA ocean models, a global model on a .5 x .7 degree grid (lat,long) and a North Pacific model (N. of 20°S) on a .25 x .35 degree grid. This is the resolution for each dependent variable. The models use detailed coastline geometry including the islands resolved by the grid. The models are reduced gravity with the lowest layer infinitely deep and at rest and they include thermodynamics and mixing. The models have been forced by the Hellerman-Rosenstein (1983) (HR) wind climatology and by winds from the European Centre for Medium-range Weather Forecasting (ECMWF) (1980-1987). The discussion will focus on the Pacific west of the dateline and ± 20 degrees latitude, including the Indonesian archipelago. The models simulate detailed aspects of the circulation in the region.

2. Mean flow and sea surface height.

Figure 1a,b shows the sea surface height (SSH) from the global model driven to statistical equilibrium by the HR monthly wind stress climatology. Between the subtropical and subpolar gyres, it shows the bifurcation of the Kuroshio/Oyashio Current system into subarctic and subtropical fronts. The frontal positions are in good agreement with those given by Roden and Robinson (1988). The simulated North Equatorial Current (NEC) is centered at 12°-13°N and the North Equatorial Countercurrent (NECC) at about 5°N similar to the U.S. Navy's GDEM climatology (Teague et al, 1989) (Fig 1c). The Mindanao eddy is simulated east of the south Philippines coast.

Figure 1b shows the annual mean SSH from the same global simulation for the western tropical Pacific. Figure 1d shows the same field from the .25° Pacific model. Both experiments have one active layer, hereafter referred to as 1.5 layers. The NEC splits at the Philippine coast into the Mindanao current and the beginning of the Kuroshio current. The location of the split shows a seasonal variation of only about 1° in the models. In the Pacific model (Fig. 1d) the mean location is in close agreement with Wyrtki (1961) and the GDEM climatology (Fig. 1c). However, the global model (Fig. 1b) has the split 1.5° further north.

A comparison of two global experiments with the south Sulu Sea open and closed shows that this occurs because the south Sulu Sea is open in the Pacific model experiment and closed in the global one. With the south Sulu Sea open there is a net cyclonic flow around the Philippines which weakens the Mindanao Current and strengthens the Kuroshio Current east of Luzon. Hence, more of the SSH contours associated with the NEC must go north when the south Sulu Sea is open and the split point must be further south. Flow through the south Sulu strait has little effect on the transports south of the Celebes Sea, east of 130°E, and north of the Luzon Strait. The mean transports for the Mindanao Current at 8°N (coast to 134.4°E) and the Kuroshio

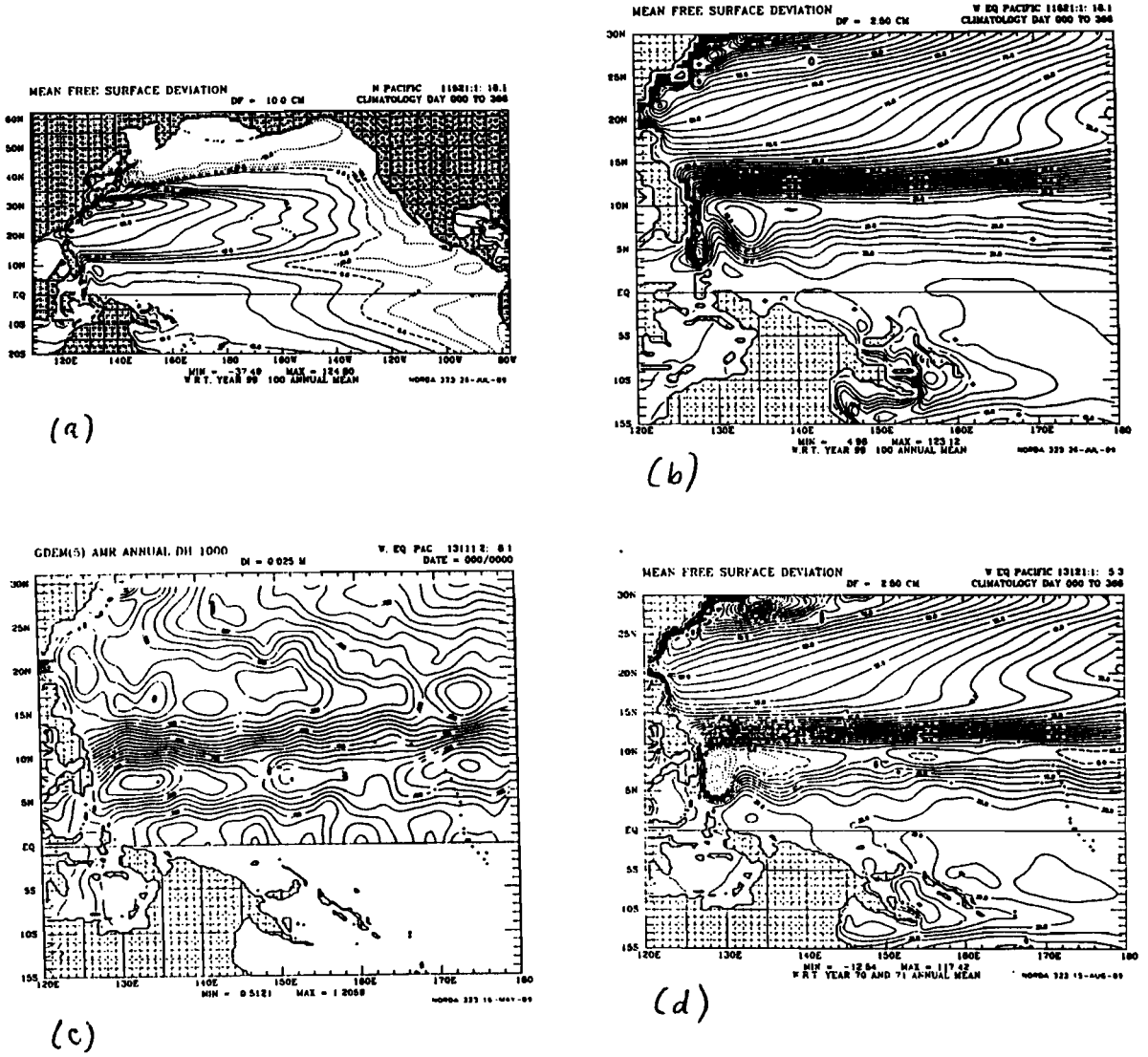

Fig. 1. (a) Mean SSH from the .5° 1.5 layer global model driven by the Hellerman-Rosenstein (HR) wind stress climatology. (b) Mean SSH for the western tropical Pacific from the same numerical experiment. (c) Annual mean surface dynamic height relative to 1000 m from the U.S. Navy's .5° GDEM climatology (Teague et al, 1989) smoothed with 5 passes of a 9-point real smoother for a spherical grid. The global areal mean from the Levitus (1982) climatology has been subtracted. (d) Same as (b) from the .25° 1.5 layer Pacific model. The model land-sea boundary is the 200 m isobath.

Current at 18°N (coast to 124.6°E) are 27 Sv, 22 Sv for the 1.5 layer Pacific model (S. Sulu open), 34 Sv, 12 Sv for the 1.5 layer global model (S. Sulu closed) and 24 Sv, 17 Sv for a 3.5 layer global experiment (S. Sulu closed).

Focusing on the global model, the Mindanao current splits near the south end of the Philippines. Some flow recirculates in the eddies. The strongest branch heads southward before joining the NECC. Wyrtki (1961) notes this branch passing between Sangihe and Talaud Islands which form a channel between 125.8°E and 126.8°E at 4°N. The configuration of the island geometry and the bottom topography (parallel ridges bounding the current) suggest that they might influence the path of the current. However, they are not included in the .5 degree global model which shows the mean current centered at 126.7°E. The Pacific model which includes the islands shows the current centered at 127.3°E and not extending as far south. The lack of Pacific-Indian Ocean throughflow and the net cyclonic flow around the Philippines with the south Sulu Sea open are likely factors in this.

In the global model another branch of the Mindanao Current proceeds westward through the Celebes Sea where some flow returns eastward north of Suluwesi Island, and some proceeds southward through the Macassar Strait. The flow through Macassar again divides into Pacific-Indian Ocean throughflow (see Kindle et al, Murray et al, this volume) and flow that returns northward east of Suluwesi and Halmahera Islands where it joins the NECC. For the latter flow, the standard deviation is larger than the mean and the mean is <1 Sv. In the model little or none of the Mindanao Current flows around the south side of Halmahera Island before joining the NECC.

In the annual mean there is a westward coastal current along the New Guinea coast in the 1.5 layer model, Fig. 2a, but in the 3.5 layer model the westward coastal current is an undercurrent with only weak mean westward flow at the surface (Fig. 2c, d). Another prominent difference between the 1.5 and 3.5 layer models occurs in the equatorial waveguide. In the 1.5 layer model the equator is roughly the southern edge of the NECC in the annual mean. In the 3.5 layer model a westward equatorial surface current and an eastward equatorial undercurrent are found. Thermodynamics was not included in the 3.5 layer simulation, but vertical mixing of mass and momentum were. The vertical mixing and at least two active layers are required for these currents to exist in the annual mean.

Figure 2b shows the effect of the Pacific-Indian Ocean throughflow on the u-component of velocity in the 1.5 layer global model. This was obtained by subtracting a solution with the Pacific-Indian Ocean throughflow closed from one with the throughflow open. In the western equatorial Pacific the throughflow influence is confined mainly to an increased westward component along the New Guinea coast and into the Celebes Sea. It also slightly weakens the Mindanao eddy and shifts the cyclonic eddy to the east of it (Fig. 1b) slightly further to the east.

The region also exhibits several prominent eddies in the annual mean SSH field (Fig. 1b, d). However the strength, location, and even existence of these is quite variable. The most notable is the cyclonic Mindanao eddy centered at 5°N, 127.5°E in the global model (Fig. 1b) and 6°N, 128.5°E in the Pacific model (Fig. 1d). A second cyclonic eddy is found to the east in both models centered at 8°N, 133°E and 9°N, 134.5°E, respectively. Additional cyclonic centers are found to the east along the SSH trough at 9°N. The longitudinal structure is in good agreement with the GDEM climatology (Fig. 1c). Both GDEM and the Pacific model show a center between 150°-155°E. A test of the Pacific model with and without the Gilbert Islands did not show any notable differences. An anticyclonic eddy is found near 3°N, 132°E, ENE of Halmahera.

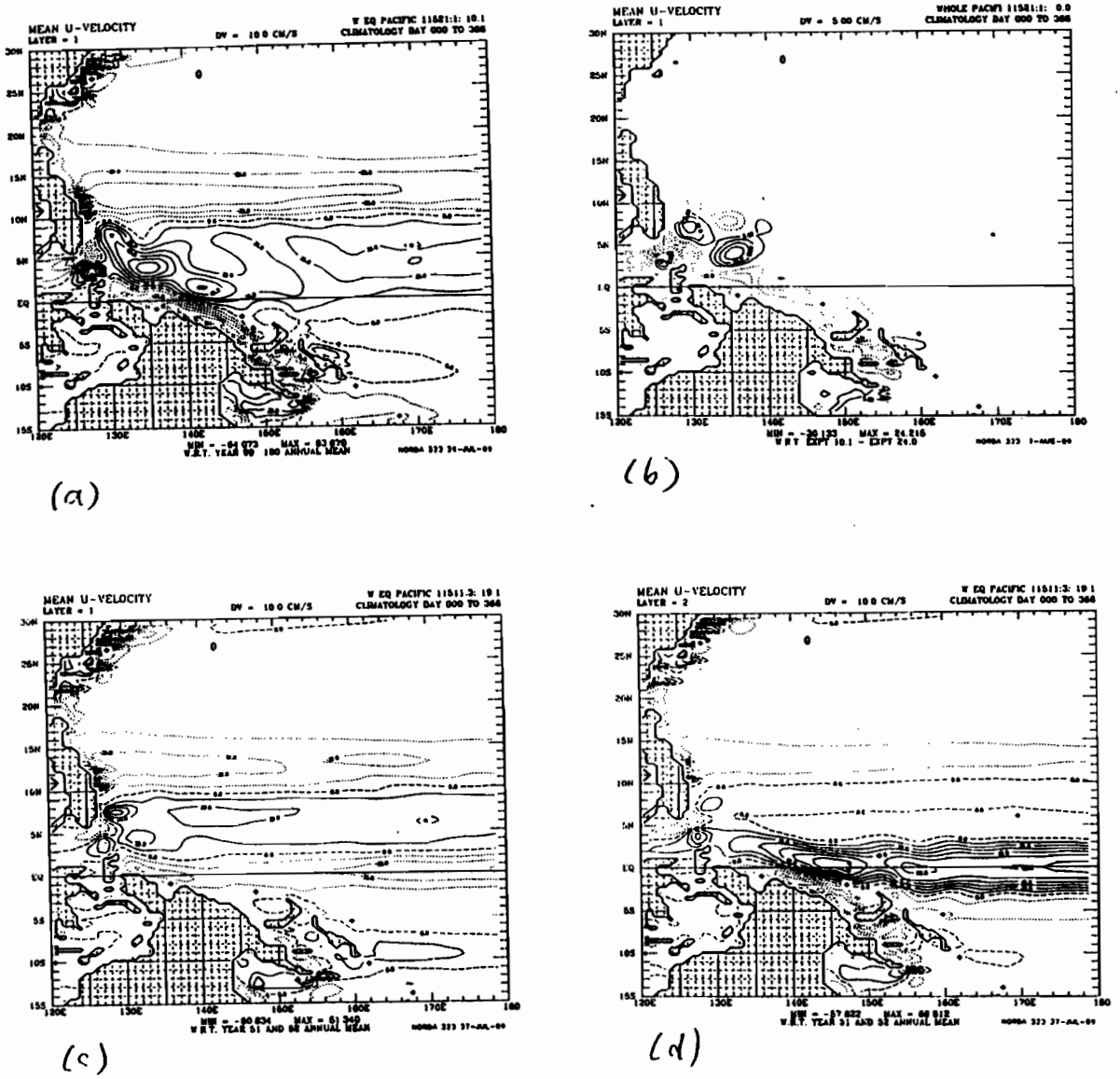

Fig. 2. Mean u-component of velocity for (a) the 1.5 layer global model, (b) the difference between two 1.5 layer global experiments, Pacific-Indian Ocean throughflow open minus Pacific-Indian Ocean throughflow via Indonesia closed, (c) layer 1 of the 3.5 layer global model, and (d) layer 2 of the 3.5 layer global model. Dashed contours are westward. HR monthly mean wind stress forcing.

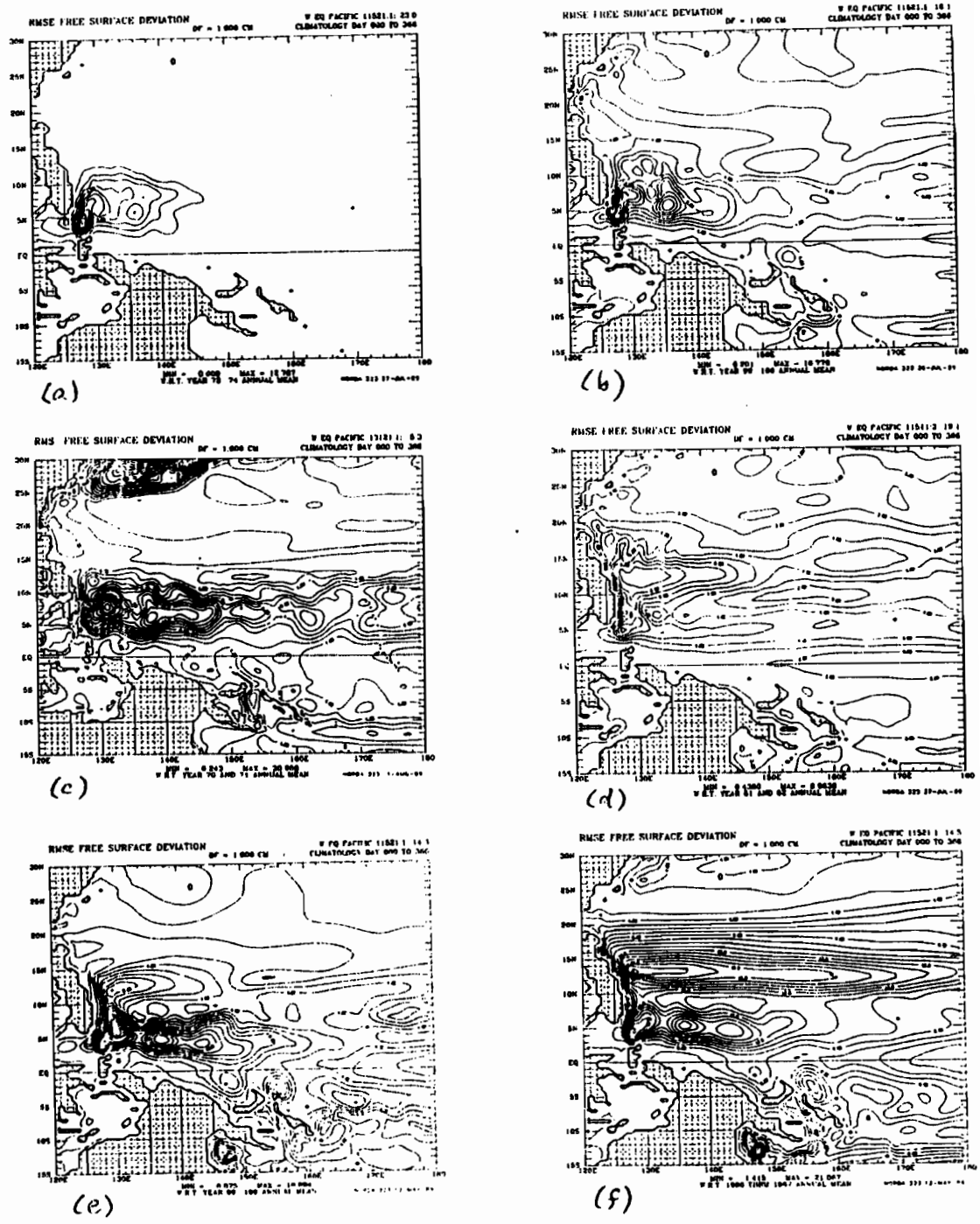

Fig. 3. RMS SSH variability from model experiments listed in Table 1. (a) .5° 1.5 layer global model driven by annual mean HR wind stress, (b) same driven by the monthly HR climatology, (c) .25° 1.5 layer Pacific model driven by the HR monthly climatology (d) .5° 3.5 layer global model driven by the HR monthly climatology, (e) the .5° 1.5 layer global model driven by a monthly 1000 mb ECMWF wind climatology based on 1980-1987 winds, and (f) .5° 1.5 layer global model driven by monthly mean 1000 mb winds for individual years from ECMWF, 1980-1987.

In the southern hemisphere cyclonic eddies are found in the Bismarck Sea and east of New Ireland. In the 3.5 layer model these eddies occur in the undercurrent layer, but unlike the 1.5 layer model, they are not found in the surface layer in the annual mean. Cyclonic eddies are also found in the Coral Sea and the Solomon Sea. Many more transient eddies are present.

3. Variability.

The RMS variability of the SSH in the western equatorial Pacific has been calculated for several different numerical experiments shown in Figure 3. The forcing and model for the experiments are listed in Table 1.

TABLE 1 - Model Experiments shown in Figure 3

Figure	Wind forcing	Model
3a	annual mean HR climatology	.5° , 1.5 layer global
3b	monthly HR climatology	.5° , 1.5 layer global
3c	monthly HR climatology	.25° , 1.5 layer Pacific
3e	monthly ECMWF climatology	.5° , 1.5 layer global
3d	monthly HR climatology	.5° , 3.5 layer global
3f	ECMWF monthly means for individual years, 1980-1987	.5° , 1.5 layer global

The ECMWF climatology is a monthly mean of 1000 mb winds 1980-1987 on a 2.5° grid. The 1000 mb winds were multiplied by a constant to produce surface winds. All of the experiments include thermodynamics except for the 3.5 layer global. Global experiments a,b use an eddy viscosity of A = 2000 m^2 s^{-1} and d-f use A = 1500 m^2 s^{-1}. The Pacific model uses A = 500 m^2 s^{-1}.

The experiments shown in Figure 3 are designed to help sort out variability due to flow instabilities, seasonal variations in winds from different wind sets and interannual variability. In Figure 3a the RMS variability is due only to flow instabilities. With only one vertical mode, baroclinic instability is excluded from all but Figure 3d. Figure 3f is the only one to include interannual variability, but some of the interannual variability may be fictitious due to changes in the ECMWF wind product over the 8-year period.

In Figure 3a, driven by annual mean winds, flow instabilities occur within 12° of the equator west of 150°E. Strongest instabilities are associated with the Mindanao eddy and the NECC. The tongue of variability into the Celebes Sea is associated with eddy shedding from the Mindanao eddy. Usually pieces of the eddy break off, but occasionally the whole eddy propagates into the Celebes Sea. The eddy shedding is irregular but occurs at roughly 40-80 day intervals. At 141°E spectral peaks in the transport 2°-5°N occur at 50-60 and 73 days in a 2-year time series. Between the New Guinea coast (2.5°S) and the equator additional peaks are found at 25 and 40 days. The Mindanao eddy itself is not one eddy, but a series of eddies that propagate in from the east and strengthen there, either merging with or replacing the Mindanao eddy. This occurs less frequently than the eddy shedding.

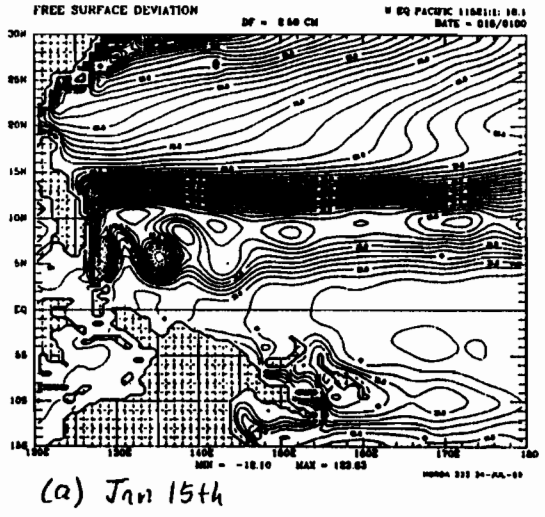

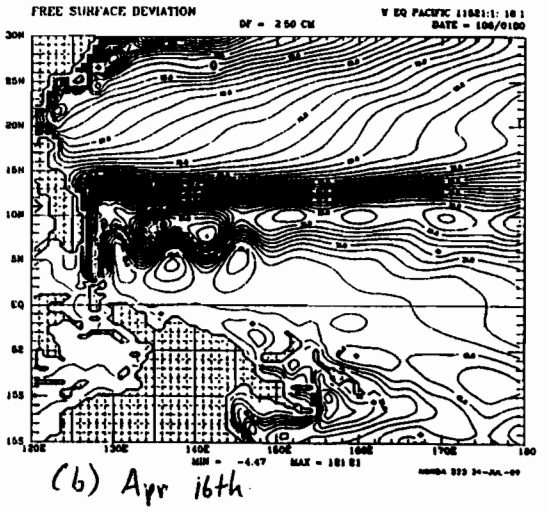

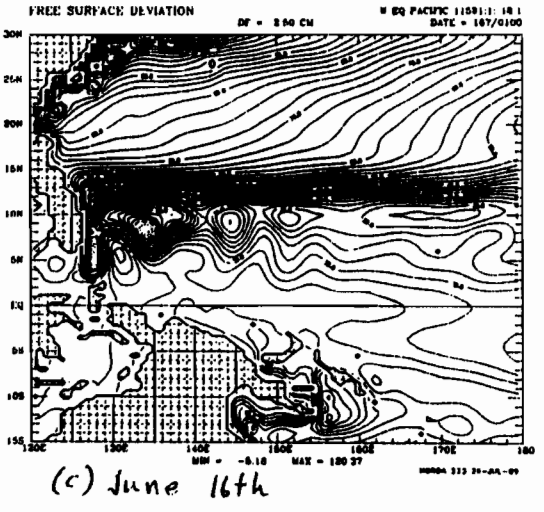

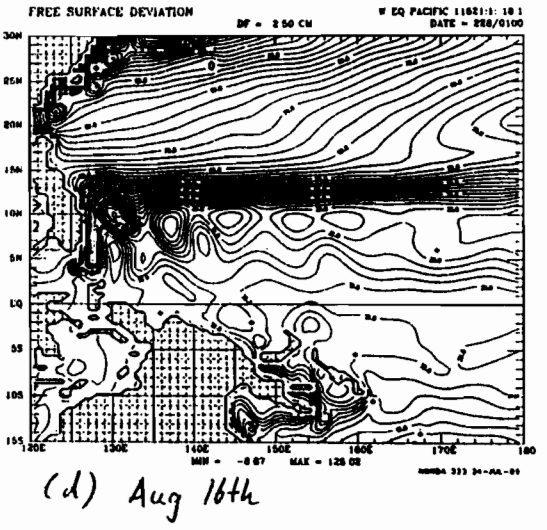

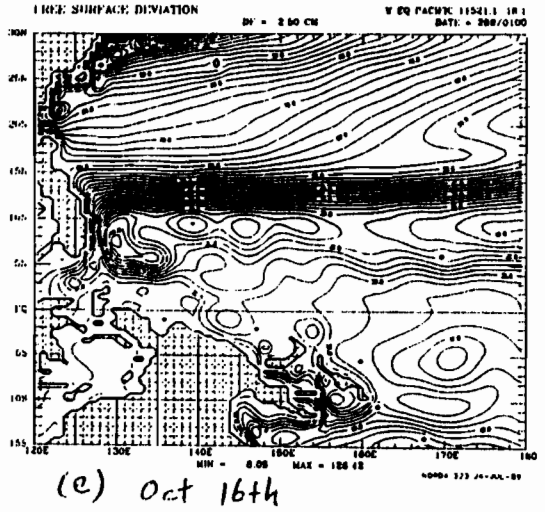

Fig. 4. Instantaneous SSH from the .5° 1.5 layer global model driven by the HR monthly wind stress climatology for (a) Jan. 15th, (b) Apr 16th, (c) June 16th, (d) Aug 16th, and (e) Oct. 16th.

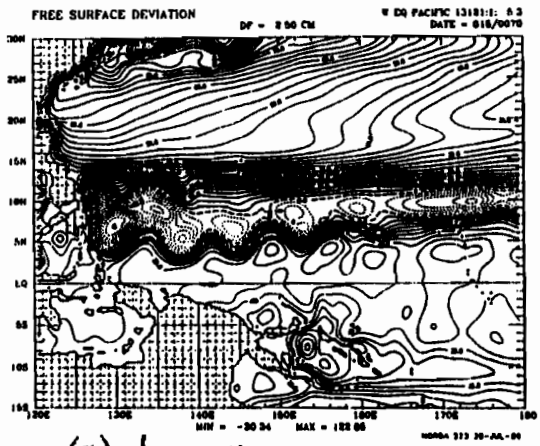

(a) Jan 15th

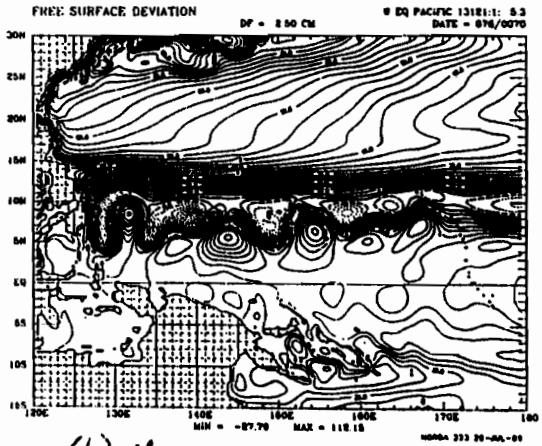

(b) Mar 17th

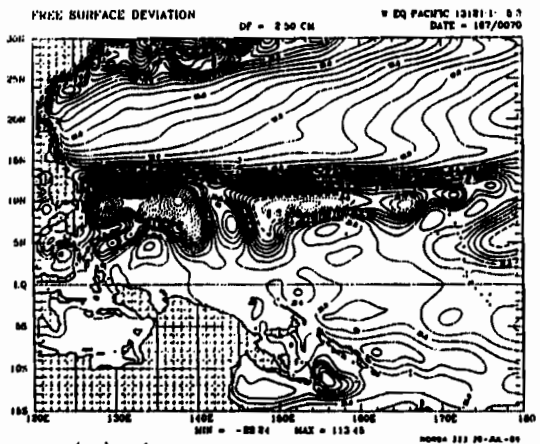

(c) June 16th

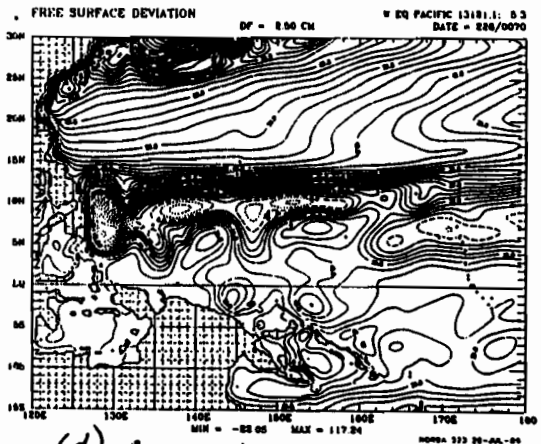

(d) Aug 16th

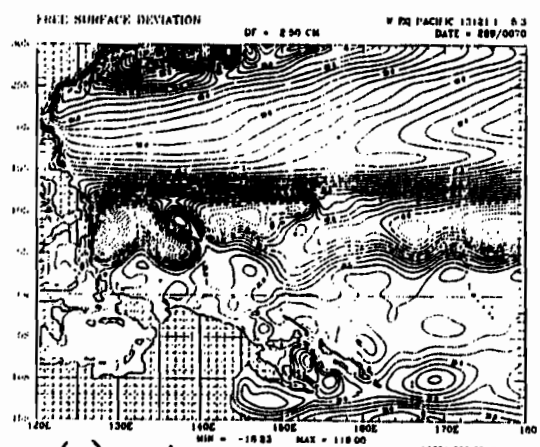

(e) Oct 16th

Fig. 5. Instantaneous SSH from the .25° 1.5 layer Pacific model driven by the HR monthly wind stress climatology for (a) Jan 15th, (b) Mar. 17th, (c) June 16th, (d) Aug 16th, and (e) Oct 16th.

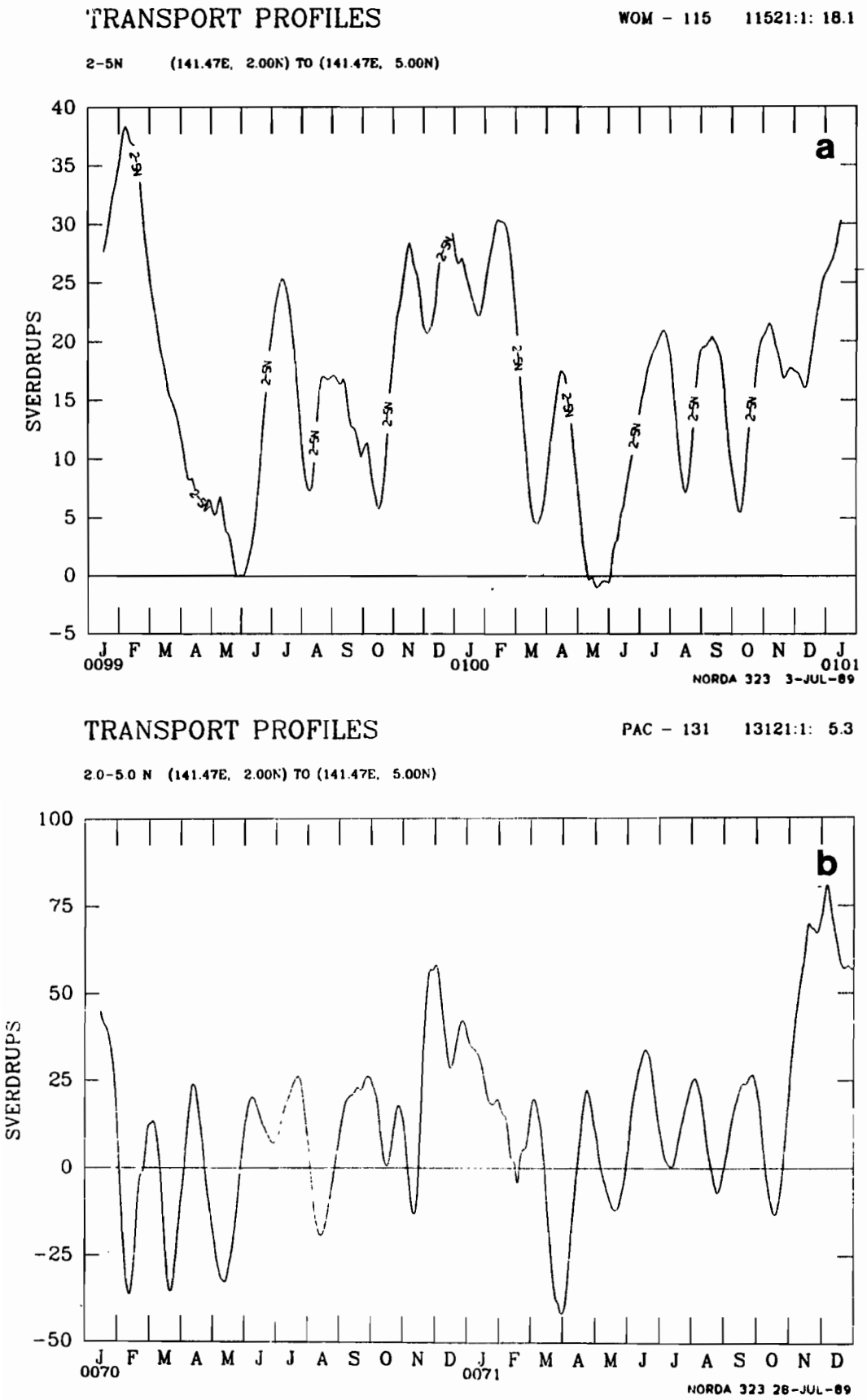

Fig. 6. Two-year transport time series from (a) the 1.5 layer global model and (b) the 1.5 layer Pacific model at 141.5°E, 2-5°N driven by the HR monthly climatology. The time series begin on Jan. 15th and ticks mark 1 month intervals.

Similar flow instabilities are found north of the equator in the western Atlantic Ocean and just south of the equator in the western Indian Ocean. The latter are discussed by Kindle and Thompson (1989) who reported similar periodicities.

Figures 3b-e driven by monthly wind climatologies all show patterns of RMS SSH variability with maxima in bands N and S of the equator. We anticipate that the minimum along the equator would disappear in maps of eddy kinetic energy (which we have not calculated yet). The longitudinal location of the variability maxima are very similar in Figures 3b, 3c, and 3e whether driven by Hellerman-Rosenstein or ECMWF winds, suggesting a standing wave. Such maxima are not clearly evident in the 3.5 layer model (Fig. 3d).

In all cases there are tongues of high variability into the Celebes Sea. Although eddy fragments break off the Mindanao eddy year round and propagate into the Celebes Sea, occasionally the whole Mindanao eddy propagates into the Celebes Sea sometime during May through October.

SSH variability maxima in the Bismarck Sea and east of New Ireland are also consistent features except in the 3.5 layer model. The eddies in the Bismarck Sea form north of the Vitiaz Strait and propagate northwestward. Similarly, eddies form east of the strait between New Ireland and the Solomon Islands from July through October. As noted earlier (Fig. 2) the mean upper layer flow is westward along the northern New Guinea coast in the 1.5 layer model, but only weakly so in the 3.5 layer model. In the 3.5 layer model there is a westward coastal undercurrent and the eddies in the Bismarck Sea and east of the New Ireland are also present only below the surface layer in the mean.

The Coral Sea is a region of high variability with the ECMWF winds, but not with the HR. Figures 3c,e,f also show variability in parts of the Solomon Sea.

The western NEC is another region of slightly to markedly elevated variability in Figures 3b-f. A striking difference between the .25° Pacific model and the .5° global model is seen north of 25°N where the .25° model shows strong flow instabilities in the Kuroshio and the .5° model does not.

The interannual variability (Fig. 3f) is larger in amplitude and more wide spread. It shows the features of the seasonal variability with elevated amplitude, but the maximum variability is associated with shifts in the latitude of the NEC. Two-year means of SSH 1980-81, 1982-83, etc. suggest that some of the interannual variability is due to changes in the ECMWF 1000 mb wind product over the years. The two-year means become distinctly more realistic with time.

4. Seasonal Cycle.

Figures 4 and 5 show the seasonal cycle of the SSH from the .5° 1.5 layer global model (Fig. 4) and the .25° 1.5 layer Pacific model (Fig. 5). Both show a similar seasonal cycle, but with more eddy activity in the Pacific model. Because of the flow instabilities, substantial interannual variation occurs in both models even though they were driven by the Hellerman-Rosenstein wind climatology, especially west of 160°E, within 10° of the equator. Jan. 15th shows the SSH gradient associated with the NECC at a lower latitude in the western part of region. By March the latitude has increased in the western part and we see the onset of strong anticyclonic eddies on the south side. These show up as 50-60 day oscillations in the transport time series at 141.5°E, 2°-5°N (Fig. 6). In summer a new trough appears at a lower latitude in the east (June 16th and Aug 16th). By Oct. 16th it has increased in latitude. This rise appears to follow the rise in latitude of the wind curl pattern. There is no obvious propagation of an annual Rossby wave associated with the increase in latitude.

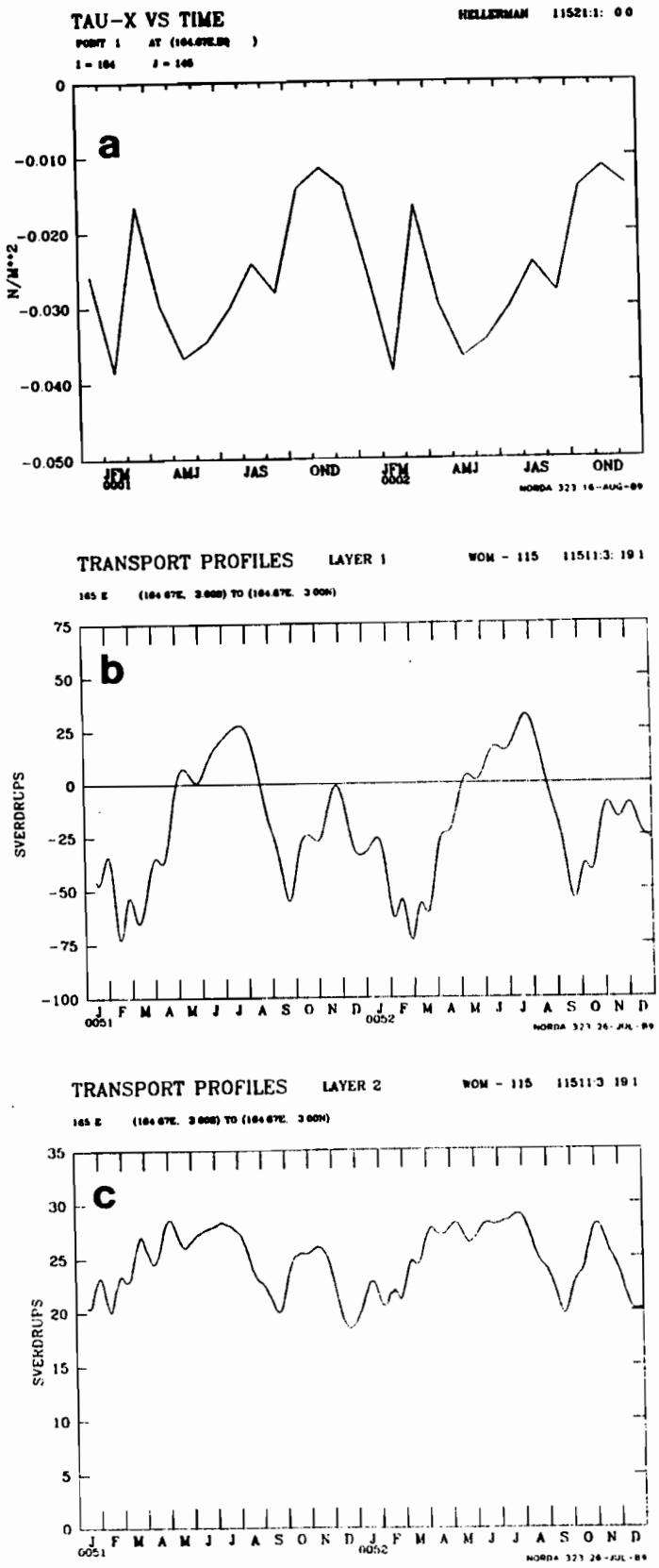

Fig. 7. Two-year time series of (a) the equatorial component of the HR wind stress climatology at 165°E, (b,c) transports of the equatorial (b) surface current in layer 1 and (c) undercurrent in layer 2 from the 3.5 layer global model. For the wind stress component the monthly average is placed midway between the ticks. The 15th of the month falls midway between the ticks in the transport time series.

Other features of the variability are also evident such as the eddy shedding into the Celebes Sea. Eddy plumes are seen north of New Britian Island. The eddy activity east of New Ireland is most pronounced in the latter part of the year. Eddy activity in the Coral and Soloman Seas is also evident. In the .25° Pacific model eddy activity (north of 25N°) is associated with the Kuroshio.

Figure 7 shows time series of the equatorial surface current and undercurrent from the 3.5 layer global model at 165°E. For comparison the equatorial u-component of the HR wind stress for 165°E is also shown.

Strong 30-day oscillations are evident with onset in winter and late summer. The oscillations are nearly in phase in the two layers. Although the surface current and undercurrent tend to be opposite in direction, their transport tends to accelerate in the same direction.

Acknowledgements. The authors would like to thank Pat Hogan, Bill Teague, Amy Summers and Greg Vega for their assistance on this project. The computations were performed on the CYBER 205 at Fleet Numerical Oceanography Center in Monterey, CA. We would like to thank Dana Thompson, George Heburn and Robert Woodyard for their contributions to the developmental work. The manuscript was typed by Debbie Black. Approved for public release; distribution is unlimited. NORDA Contribution #PR-89:059:323.

REFERENCES

Hellerman, S., and M. Rosenstein, 1983: Normal monthly wind stress over the world ocean with error estimates. *J. Phys. Oceanogr.*, **13**, 1093-1104.

Kindle, J.C., H.E. Hurlburt, and E.J. Metzger, 1989: On the seasonal and interannual variability of the Pacific to Indian Ocean throughflow. (this volume).

Kindle, J.C., and J.D. Thompson, 1989: The 26 and 50-day oscillations in the western Indian Ocean: Model Results. *J. Geophys. Res.*, **94**, 4721-4736.

Levitus, S., 1982: Climatological atlas of the world ocean. NOAA Professional Paper 13, 173 pp.

Murray, S.P., J.C. Kindle, D. Arief, and H.E. Hurlburt, 1989: Comparison of observations and numerical model results in the Indonesian throughflow region. (this volume).

Roden, G.I., and A.R. Robinson, 1988: Subarctic frontal zone in the northeastern Pacific: mesoscale structure and synoptic description. Reports in Meteorology and Oceanography #31, Harvard University.

Teague, W.J., M.J. Carron, and P. Hogan, 1989: A comparison between the GDEM and Levitus climatologies. (Submitted to JGR-Oceans).

Wyrtki, K., 1961: Physical Oceanography of the southeast Asian waters. NAGA Report #2, Scripps Inst. Oceanogr., 195pp.

WESTERN PACIFIC INTERNATIONAL MEETING AND WORKSHOP ON TOGA COARE

Nouméa, New Caledonia
May 24-30, 1989

PROCEEDINGS

edited by

Joël Picaut *
Roger Lukas **
Thierry Delcroix *

* ORSTOM, Nouméa, New Caledonia
** JIMAR, University of Hawaii, U.S.A.

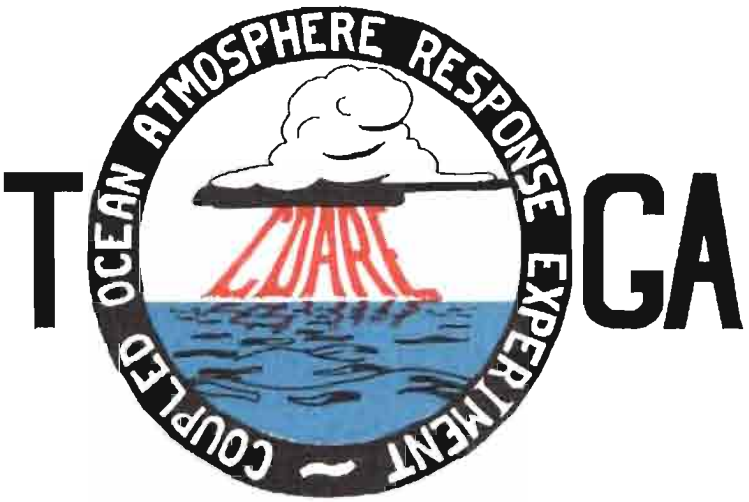

INSTITUT FRANÇAIS DE RECHERCHE SCIENTIFIQUE
POUR LE DÉVELOPPEMENT EN COOPÉRATION

ORSTOM

Centre de Nouméa

TABLE OF CONTENTS

MEETING COLLECTED PAPERS

WATER MASSES, SEA SURFACE TOPOGRAPHY, AND CIRCULATION

EL NINO/SOUTHERN OSCILLATION 1986-87

THEORETICAL AND MODELING STUDIES OF ENSO AND RELATED PROCESSES

MOMENTUM, HEAT, AND MOISTURE FLUXES BETWEEN ATMOSPHERE AND OCEAN

EMPIRICAL STUDIES OF ENSO AND SHORT-TERM CLIMATE VARIABILITY